Check for updates

Detection of unlabeled nanoplastics within *Daphnia magna* using enhanced darkfield hyperspectral microscopy

Arav Saherwala,[a] Jun-Ray Macairan,[a] Emma Geoffroy[a] and Nathalie Tufenkji (ID) *[ab]

The ubiquity of small plastic particles in the environment compels researchers to better understand their ecotoxicity, hence motivating the need for advanced methods to localize plastic particles within whole organisms. Nanoplastics ($< \sim 1$ μm) have proven particularly challenging to detect due to their small size, which has limited our understanding of their potential for biouptake and subsequent impacts. To address this research gap, this work focuses on detecting internalized plastic particles in a model freshwater organism (*Daphnia magna*) using a combination of histology and enhanced darkfield hyperspectral imaging (EDF-HSI). A cryotome was used to obtain histological slices of the whole organism and minimize the interference of biological tissue that impairs the visualization of plastic particles. Furthermore, this study presents a method to modify the spectral response of biomass using hematoxylin and eosin staining. The incorporation of the staining protocol with EDF-HSI enables the detection of ingested plastic particles, such as polystyrene, polyethylene, polymethyl methacrylate, polyvinylchloride, and polytetrafluoroethylene. The results demonstrate the detection of nanoplastics as small as 500 nm at low exposure concentrations (0.01 ppm). A key advantage of this method is that plastics do not need to be pre-labeled prior to internalization by organisms. This makes it a promising methodology for ecotoxicology studies since ingested unlabeled microplastics and nanoplastics can be localized inside an organism. The proposed method using EDF-HSI combined with biomass staining to analyze histological slices for the localization of nanoplastics within whole organisms will aid in improving our understanding of the fate and impacts of plastic pollution.

Environmental significance

Degradation of plastic waste can lead to the increased consumption of microplastics and nanoplastics by organisms. To better understand the toxicological impact of these particles, established protocols to detect microplastics and nanoplastics within whole organisms are needed. This study proposes a method to detect nanoplastics within a model organism by combining enhanced darkfield hyperspectral imaging and histological techniques. A post-exposure staining protocol is used to differentiate biomass from internalized plastic particles. This approach enables the detection of plastic particles as small as 500 nm at environmentally relevant exposure concentrations, thereby offering a new approach to understanding the growing concern of nanoplastic toxicity.

Introduction

Plastic pollution is ubiquitous, affecting both aquatic and terrestrial environments. In the natural environment, bulk plastic items can break down into smaller microplastics (~ 1 μm to 5 mm)[1] and nanoplastics (smaller than ~ 1000 nm)[2] due to mechanical, chemical, and biological degradation. Small plastic particles have been detected in different bodies of water, including freshwater,[3–5] marine waters,[6,7] and in uninhabited locations, such as high-altitude Alps[8] and the Tibetan Plateau.[9] The ubiquity of microplastics and nanoplastics has motivated the need to better understand their ecotoxicity and environmental fate.[10] Once microplastics and nanoplastics are introduced into the environment, they can be ingested by organisms, where the plastic particles can then bioaccumulate through the food chain.[11] The ingested plastic particles can cause damage to internal organs, such as the digestive tract.[12] Moreover, nanoplastic toxicity can differ from that of microplastics.[13,14] The smaller size of nanoplastics enables cellular internalization.[15] Therefore, it is crucial to understand the mechanisms of nanoplastic biouptake as they can be more hazardous than the microplastic fraction.[16] For example,

[a] *Department of Chemical Engineering, McGill University, Montreal, Quebec H3A 0C5, Canada. E-mail: nathalie.tufenkji@mcgill.ca; Tel: 514 398 2999*
[b] *United Nations University Institute for Water, Environment and Health, Richmond Hill, Ontario, L4B 3P4, Canada*

localizing ingested plastic particles within whole organisms can help improve our understanding of changes in hormones, morphology, behaviour, and reproduction.[17,18] Accordingly, adequate methods are needed to detect microplastics and nanoplastics within exposed aquatic and terrestrial organisms.

Numerous analytical techniques exist to characterize microplastics and nanoplastics. For instance, pyrolysis gas chromatography mass spectrometry (pyro-GC-MS) enables chemical identification of particles.[19] However, the destruction of the sample in pyro-GC-MS results in a loss of spatial information, and thus, the inability to localize particles within exposed organisms. Vibrational techniques, such as μRaman and micro-Fourier-transform infrared (μFTIR) spectroscopy, are the most commonly used analytical tools for identifying microplastics.[20,21] For example, μFTIR has been used to assess microplastic contamination in mussels,[22] and oysters.[11] However, μFTIR is often limited to identifying microplastics larger than 20 μm, and the presence of natural organic matter can interfere with spectral analysis for both Raman and FTIR spectroscopy.[23] Novel spectroscopy methods, such as atomic force microscopy-infrared and surface-enhanced Raman spectroscopy, have been used to detect nanoplastics in environmental samples.[7,24] More recently, hyperspectral imaging (HSI), a label-free, non-destructive, and rapid method, has been used for detecting and identifying microplastics.[25,26] This imaging modality uses visible or near-infrared light to acquire a whole spectrum for every pixel from a sample image. The combination of acquiring spatial information and spectral data is advantageous for environmental characterization. For example, HSI has been used to characterize microplastics collected in the Po River, Italy,[27] as well as spiked microplastics within dissected intestinal tracts of fish,[28] digested mussel tissue,[29] and agricultural soil samples.[30] However, due to the lower resolution of conventional HSI, it has mainly been used to characterize microplastics larger than ~100 μm.[25,26,31,32] It is worth noting that conventional analytical techniques used for detecting and identifying microplastics and nanoplastics within biological samples often require extensive sample pre-treatment, such as digestions to remove organic matter that can interfere with spectrum acquisition.[33] However, several digestion techniques use harmful solvents that can melt,[34] decompose,[35] or discolour[36] plastics in the sample. Moreover, sample digestion impacts the spatial distribution of plastic particles in the sample due to its destructive nature. To further the understanding of microplastic and nanoplastic ecotoxicity and environmental fate, it is crucial to use methodologies that preserve the sample integrity while enabling the detection of these contaminants of emerging concern.

Alternative methods to study ingested plastics while retaining spatial information have been developed. For example, fluorescent dyes are often applied to particles prior to organism exposure, resulting in the organism of interest ingesting labeled particles.[37,38] However, the size, shape, and surface properties of commercially available fluorescent particles are not always environmentally relevant. Moreover, dyes can leach from the particles, resulting in the misidentification of particles or false positives.[39] The leached dye may also pose potential toxicity to the organism, making it difficult to determine the actual cause of organism toxicity.[40]

To address the need for nanoplastic localization in environmental samples, we have developed a methodology that relies on post-exposure staining to detect nanoplastics using enhanced darkfield hyperspectral imaging (EDF-HSI) in combination with histology. For the detection of smaller particles, EDF-HSI has been proposed for its higher signal-to-noise ratio[41] enabling the detection of silver nanoparticles (>10 nm) in water samples,[42,43] polymer-coated gold/copper sulfide nanoparticles (>25 nm) in human cells,[44] and gold nanoparticles (>15 nm) in *Daphnia magna* (*D. magna*).[45] EDF-HSI has also been used to detect polystyrene microplastics in matrices such as human cells[46] and *Caenorhabditis elegans* (*C. elegans*).[47] Furthermore, the ability of EDF-HSI to capture spatial information in combination with hyperspectral data is advantageous for the automatic detection of plastic particles over manual detection (*i.e.*, visual inspection). To mitigate biomass interference while preserving the organism's structure, we propose using histology, which uses microtomy or cryotomy, to acquire slices of a sample that are a few micrometres thick. Some studies have used histology to visually detect microplastics within muscle tissues[48] and *Mytilus galloprovincialis*[49] using optical microscopy. In this study, we present the combined use of cryotomy techniques with EDF-HSI to enhance the visualization and detection of microplastics and nanoplastics ingested by organisms. To effectively differentiate between biomass and plastic particles, hematoxylin and eosin (H&E) staining is applied to the whole organism after plastic particle exposure. This dye has a specificity for biomass that changes its spectral response, thereby enabling the differentiation of biomass from plastic. Hematoxylin is a basic dye that binds to negatively charged cell components, such as nucleic acids, whereas eosin is an acidic dye which binds to positively charged components, such as collagen and some amino acids.[50,51] H&E stains are both hydrophilic stains, and the hydrophobic nature of plastic particles can limit staining of plastics. Furthermore, H&E stains are the standard stain used in many histopathology and ecotoxicology studies.[52] Hence, using H&E staining would enable researchers to apply the proposed methodology in this study without major modifications to the established protocols for H&E staining. While previous studies have used H&E staining to study the histological damage to tissues caused by plastic ingestion,[48,53] this strategy has not previously been used to enable discrimination of plastic particles from biomass. Therefore, this study aims to (i) visualize nanoplastics within a whole organism using a cryotome and EDF-HSI with *D. magna* as the model organism; (ii) detect nanoplastics within

the whole organism using a post-exposure staining process with H&E staining; (iii) apply the methodology to localize different polymer types within an organism exposed to environmentally relevant concentrations of nanoplastics.

## Materials and methods

Materials

Unlabeled polystyrene (PS) particles sized 750 nm and 500 nm (07309-5 and 09836-5), 200 nm polytetrafluoroethylene (PTFE) particles (21539-100), and polymethyl methacrylate (PMMA) particles with a size distribution of 1 to 10 μm (19130-10) were purchased from Polysciences Inc. Polyethylene (PE) particles with an average size of 3 μm (140411-1) were purchased from Cospheric, and ~63 μm polyvinylchloride (PVC) particles (81388-2506) were purchased from Sigma-Aldrich. Because of their density, the pristine PE particles do not remain well-suspended in water, which limits their biouptake. Hence, to improve bioavailability, the PE particles were suspended in deionized water and subjected to UV weathering for 14 days in an LZC photoreactor (Luzchem) fitted with UV-B light (~313 nm). This weathering was found to improve the dispersibility of the PE particles. To assess the impact of UV-weathering on EDF-HSI's ability to detect weathered nanoplastics, 500 nm PS particles were also weathered using the same protocol as the PE particle weathering. Bouin's solution, used for sample preservation, was purchased from Sigma-Aldrich (HT10132). Phosphate buffered solution (PBS) was purchased from VWR (E404). Positively charged glass slides were purchased from Fisher Scientific (1255015). Hematoxylin (HHS32) and eosin (R030340–74) were purchased from Sigma-Aldrich. Polycarbonate filters (GTBP02500) were purchased from Millipore.

D. magna exposure

D. magna was chosen as the model organism as it is commonly used in microplastic and nanoplastic ecotoxicological studies.[54] Environment and Climate Change Canada (SPE1/RM/14, 2000) guidelines for maintaining the *D. magna* culture were followed. *D. magna* was cultured in moderately hard reconstituted water (comprising 60 mg L^{-1} MgSO$_4$, 96 mg L^{-1} NaHCO$_3$, 4 mg L^{-1} KCl, 60 mg L^{-1} CaSO$_4$·2H$_2$O, 2 mg L^{-1} Na$_2$SeO$_4$, and 2 mg mL^{-1} vitamin B12 in type 3 deionized (DI) water) in glass beakers. The beakers were kept in an incubator (Panasonic, MLR-352) at 20 °C with a 16/8 h day/night cycle. The culture was fed with cultured green algae (*Chlorella vulgaris*) and yeast-cerophyl-trout mix (Arofish, USA).[55]

Adult *D. magna* (7 days old) were separately exposed to 0.1 ppm of 750 nm and 0.01 ppm of 500 nm, unlabeled PS under acute toxicity conditions (48-hour exposure). *D. magna* were also separately exposed to 1 ppm of 3 μm PE particles, 0.1 ppm of 200 nm PTFE particles, 10 ppm of 63 μm PVC particles, and 1 ppm of 1–10 μm PMMA particles. Here, the
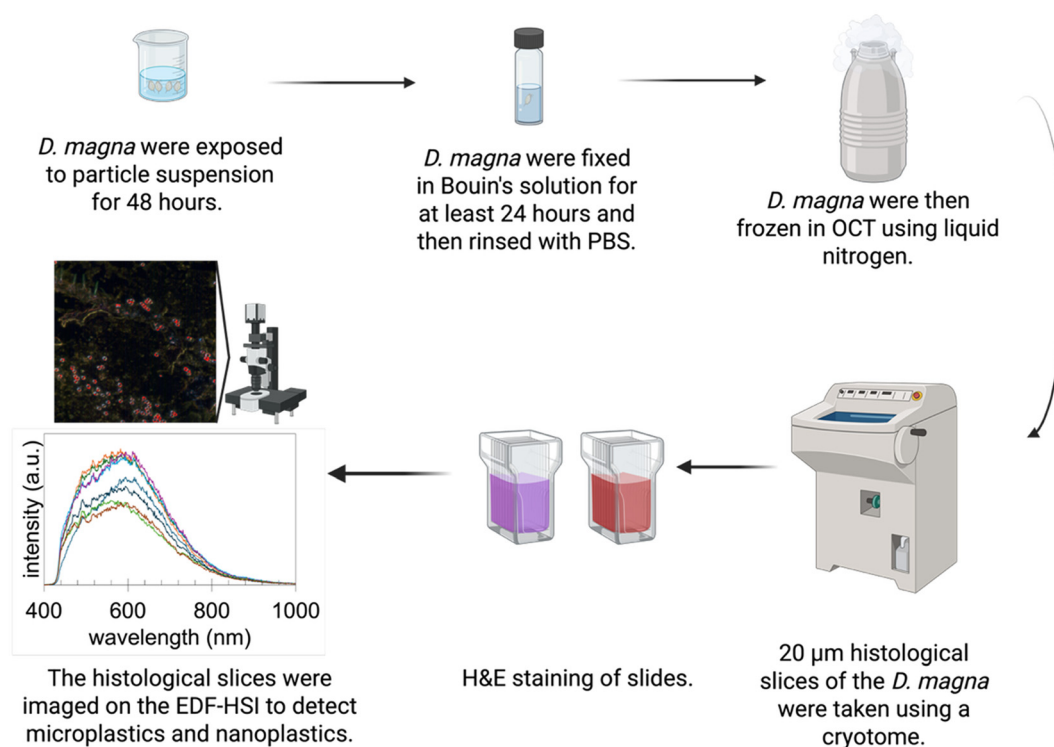
Fig. 1 Schematic of the overall procedure to obtain histological slices, subsequent H&E staining, and image acquisition. Created in BioRender. Saherwala, A. (2025) **https://BioRender.com/1jvjc4l**.

D. magna were exposed to particle suspension for 48 hours.

D. magna were fixed in Bouin's solution for at least 24 hours and then rinsed with PBS.

D. magna were then frozen in OCT using liquid nitrogen.

20 μm histological slices of the *D. magna* were taken using a cryotome.

H&E staining of slides.

The histological slices were imaged on the EDF-HSI to detect microplastics and nanoplastics.

Paper

500 nm PS at 0.01 ppm serves as the challenging environmentally relevant condition (smallest particles tested at the lowest concentration).[56] For each exposure condition, particles were separately suspended in moderately hard reconstituted water. Five adult *D. magna* were added into 50 mL glass beakers containing 40 mL of the respective treatment suspensions. The beakers were kept in a temperature-controlled incubator (Panasonic, MLR-352) at 20 °C for 48 h with a 16/8 h day/night cycle for the duration of their exposure. After exposure, *D. magna* were preserved in Bouin's solution for at least 24 h, where the organisms perished. Fig. 1 illustrates an overview of the methodological workflow.

Obtaining cryotome slices

After preservation in Bouin's solution, adult *D. magna* were rinsed with PBS, then embedded in optimal cutting temperature (OCT) resin (Sakura, 4583), and frozen in liquid nitrogen. A cryotome (McGill University, Multi-Scale Imaging Facility, Leica 3050 s) was then used to obtain transverse histological sections of the *D. magna*. The cryotome was thoroughly cleaned using acetone prior to sectioning. The chamber and sample holder temperatures were set to −25 °C. Each histological slice was 20 μm thick. While 5 *D. magna* were exposed for each treatment, only 3 were arbitrarily selected for slicing. Of those slices, at least 3 slices (collected on positively charged slides) per treatment were imaged. Each histological section was flash-dried onto the slides. Images of additional slices are found in the SI.

Staining of histological slices

To distinguish biomass from the plastic particles, an H&E staining protocol was used. Hematoxylin stains nucleic acids and ribosomes, whereas eosin acts as a counterstain, staining cytoplasmic components and is commonly used for histopathology.[57,58] Prior to staining, OCT was removed from the slides and samples were rehydrated by submerging the samples in decreasing ethanol concentrations (100%, 75%, 50% and then DI water) for 1 minute per concentration. Next, H&E stain was used to stain the histological slices at different concentrations (100%, 50%, 25%, 10%, and 5% v/v) to establish the optimal stain concentration. The staining protocol was adapted from Feldman and Wolfe.[58] First, the slides were submerged in hematoxylin at the selected concentration for at least 30 s. Following that, the slides were submerged in DI water for 30 s. Next, the slides were stained with eosin at the selected concentration for at least 90 s (in all cases, hematoxylin and eosin were used at a 1 : 1 volume ratio in DI water). Immediately after staining was completed, the slides were immersed in decreasing ethanol concentrations (100%, 75%, 50% and then DI water) for at least 1 min per concentration to prevent drying prior to imaging. Staining and rehydration were completed at room temperature. Histological slices were imaged in darkfield mode on a stereomicroscope (Olympus SZX16) before and after staining to visually confirm that the staining protocol has labelled the histological slice.

Control experiment to confirm stain selectivity.

The plastic types used for exposure (PS, PP, PTFE, PVC, and PMMA) were separately stained using H&E at a concentration of 25% v/v. First, a 200 nm polycarbonate filter (Millipore GTBP02500) was placed in a syringe filter holder and rinsed three times with 20 mL of DI water. Next, 1 mL of the respective plastic particle suspension at a concentration of 100 ppm was filtered through the polycarbonate filter. Once the particles were retained onto the filter surface, 25% v/v hematoxylin stain was filtered through the filter for 30 seconds, after which 25% v/v eosin stain was filtered for 90 seconds. After H&E staining, DI water was passed through the filter until the filtrate was clear. The filter was backwashed using 10 mL of DI water to collect the plastic particles in the retentate. Subsequently, 25 μL of the collected retentate was deposited onto a glass slide and left to dry. After the glass slide was dried, it was fitted with a cover slip with one drop of type 1 immersion oil. Then, the slide was imaged using EDF-HSI.

### Imaging and analysis using EDF-HSI.

The EDF-HSI microscope is fitted with an Olympus BX41 upright microscope, CytoViva® high-aperture darkfield condenser (CytoViva Inc., USA), and Olympus 10×, 60×, and 100× objective lenses, which were used to capture optical and hyperspectral images. A halogen bulb (International Light Technologies L1090) was fitted into the light source (Fiber Lite DC-950) and connected to the light guide. Spectral information was captured using a spectrophotometer (Specim, ImSpector V10E). ENVI 4.8 software was used to capture images at an exposure time of 250 milliseconds using 696 lines, providing a full field of view. Spectra were captured in the visual near-infrared region of 400 nm to 1000 nm at a 2 nm resolution. Spatial information in the *x-y* plane and hyperspectral data in the *z*-plane are stored in a hypercube in the ENVI 4.8 software.

Reference libraries for each of the pristine (unstained) PS, PE, PMMA, PTFE, and PVC particles suspended in DI water were created using the region of interest tool to obtain the spectra of 30–40 pixels. In Fig. S1, the darkfield images of the reference plastic types can be observed. The reference library was used to detect particles of interest within the sample images using the Spectral Angle Mapping tool. A matching angle of 0.085 radians was used. All spectra in this study are the normalized average spectra of 50 pixels from the figure of interest.

Results and discussion

Visualizing nanoplastics within *D. magna*

The first objective was to demonstrate the visualization of nanoplastics within a whole organism using cryotome
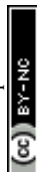
techniques and EDF-HSI. In Fig. 2A, a representative microscope image of *D. magna* can be observed prior to obtaining histological slices. After cryotomy, the histological sections of exposed *D. magna* are obtained (Fig. 2B). Here, the gut region of *D. magna* can be identified on the histological slice, as shown in green outline in Fig. 2B. Next, EDF-HSI was used to acquire hyperspectral images to visualize the ingested nanoplastic (750 nm PS), as demonstrated in Fig. 2C and D. Additional examples of microscope images showing localization of 750 nm PS nanoplastics within a whole organism can be observed in Fig. S2 and S3.

Detecting nanoplastics with optical microscopes is more challenging than detecting microplastics due to the diffraction limit of light.[59] EDF-HSI's high signal-to-noise ratio has overcome this challenge and enabled the detection of nanoparticles as small as 10 nm.[42] However, the presence of biomass in a sample can interfere with EDF-HSI's ability to acquire the spectral signal used to detect plastic particles. For example, larger and thicker samples can block the microscope's light source from passing through the sample, resulting in the inability to acquire images. Studies have demonstrated the use of histology (*e.g.*, cryotome and

microtome techniques) that effectively reduced the interference from the tissue and biomass while preserving the organism's structure to detect microplastics.[49,60–62] However, the detection of nanoplastics within a whole organism using cryotome techniques is limited in literature. In this study, the combination of EDF-HSI and cryotomy enabled the detection of unlabeled nanoplastics within *D. magna* (Fig. 2D). This combination overcomes the limitations imposed by the small size of the plastic particles and biomass interference.

Fig. 2E shows that the spectra for PS and biomass exhibit similar signatures in terms of shape and peak maxima. This similarity can lead the Spectral Angle Mapping tool to misinterpret biomass as plastic particles. Indeed, we see that some biomass (shown with the orange arrows in Fig. 2C and D) was misidentified as plastic. To mitigate this limitation, one study used pigmented microplastics to detect and identify microplastics within *C. elegans*.[47] The pigmented plastics resulted in a unique spectrum for each plastic type, enabling the identification of the microplastics using the spectral angle mapping tool. To build on the findings of Nigamatzyanova and Fakhrullin,[47] this study will stain the organism with the aim of modifying the biomass spectral
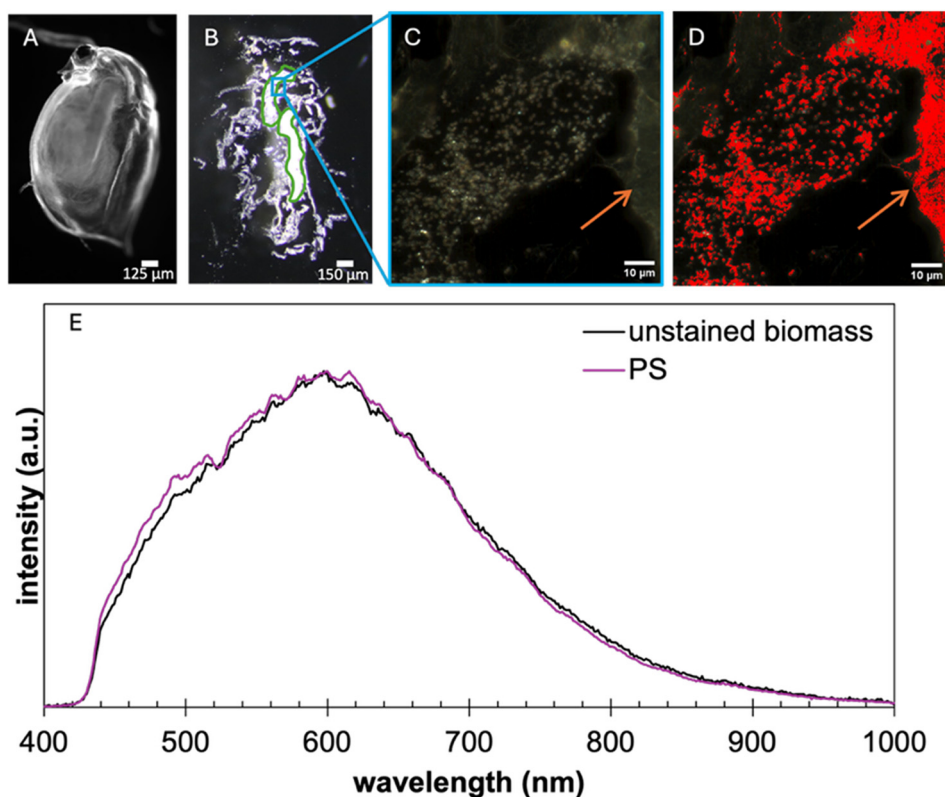
Fig. 2 Detection of 750 nm PS within a whole unstained organism. Fig. 2A depicts a darkfield image of *D. magna* acquired on an optical microscope. Fig. 2B is a 20 μm thick histological slice of a *D. magna* exposed to 750 nm PS at 0.1 ppm. The gut region of the *D. magna* is outlined in green. Fig. 2C is a darkfield image acquired on the EDF–HSI microscope. This image is taken in the gut region, as shown by the blue box. The orange arrow points to an area where only biomass is present. Fig. 2D shows the Spectral Angle Mapping of the darkfield image taken in Fig. 2C. Areas in red indicate where the spectra matched the reference spectra for PS. Fig. 2E is the normalized average spectrum of 50 pixels of biomass from Fig. 2C, and the normalized average spectrum of 50 pixels of 750 nm PS from Fig. 2C. The peak wavelength for unstained biomass is 597 nm, and the peak wavelength for PS within the histological slice is 600 nm.

response, while leaving the spectra of the particles mostly unchanged. Accordingly, an H&E staining protocol was implemented to effectively differentiate biomass from plastics.

Staining histological slices for improved nanoplastic detection

Different ratios of the H&E stain were evaluated in an effort to optimize the staining procedure for enhanced discrimination of nanoplastics from biomass using spectral angle mapping (Fig. 3). All concentrations of H&E stain resulted in a change to the biomass spectrum's shape and peak wavelength (Fig. 3A). However, the change in the spectrum's shape is considerably less pronounced for 5% and 10% concentrations compared to 25%, 50%, and 100% concentrations. Additionally, the 5% and 10% staining

caused a smaller red shift relative to higher staining concentrations (at 0%, the peak wavelength is 596 ± 1 nm; at 5%, the peak wavelength is 622 ± 12 nm, and at 10%, the peak wavelength is 631 ± 14 nm). The smaller red shifts for 5% and 10% staining were more prone to misidentifying plastic (Fig. 3E and G). In contrast, 25%, 50%, and 100% concentrations resulted in a larger red shift of the biomass' spectrum (peak wavelengths at 656 ± 1 nm, 666 ± 15 nm, and 666 ± 7 nm, respectively). Additionally, the spectrum shape at 25%, 50%, and 100% concentrations of H&E staining resulted in two peaks compared to the single peak observed at 0%, 5%, and 10% staining. Therefore, these changes at higher staining concentrations (25% staining or higher) can be used to effectively differentiate between biomass and plastic spectra.

At higher stain concentrations of 50% and 100%, some plastic particles could be inadvertently stained by excess dye
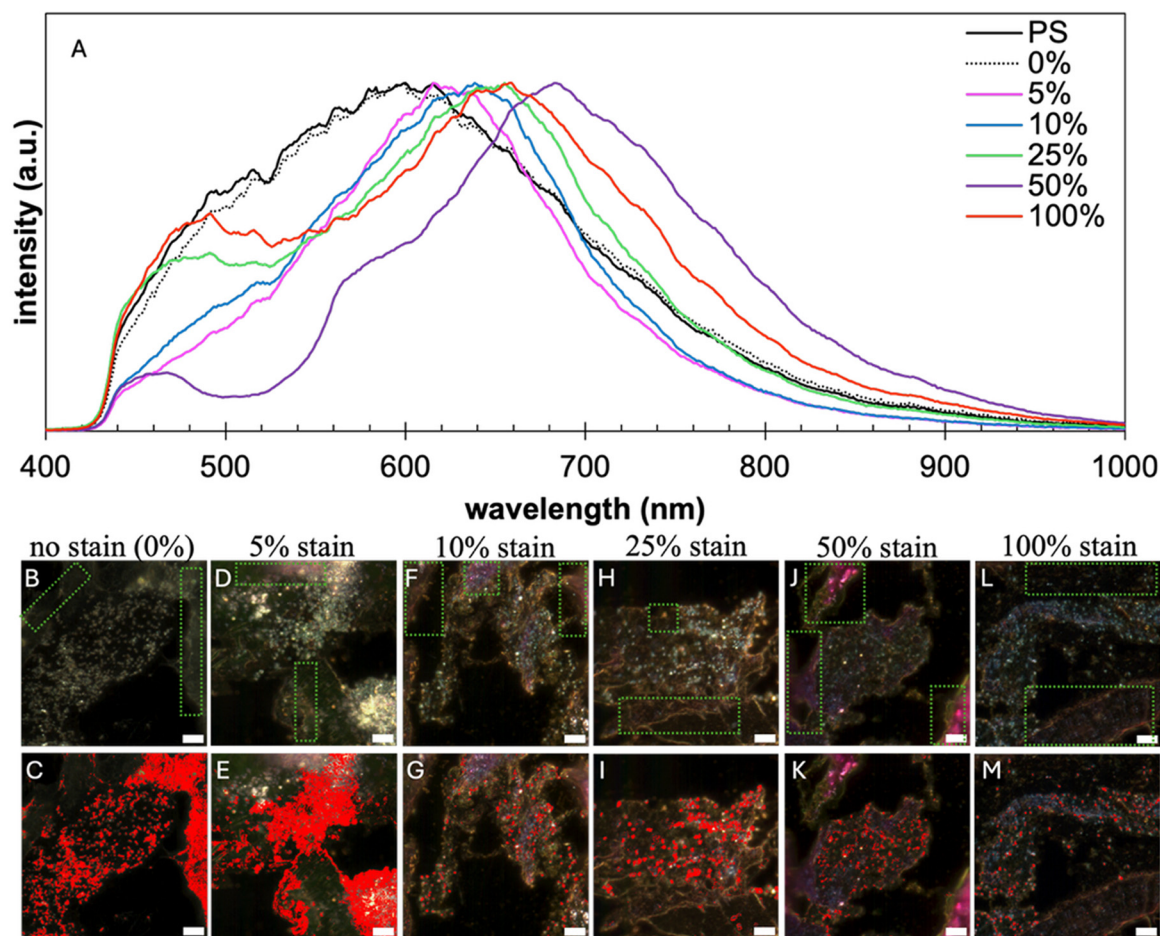
Fig. 3 H&E staining of histological slices at different stain concentrations. All *D. magna* were exposed to 750 nm PS at 0.1 ppm, and all histological slices were 20 μm thick. Fig. 3A presents the normalized average spectrum of 50 pixels of biomass from each histological slice from Fig. 3B, D, F, H, J, and L (scale bar: 10 μm). The normalized average spectrum of 50 pixels of reference PS in a histological slice is also presented in Fig. 3A (solid black). Fig. 3B is unstained, and the corresponding Spectral Angle Mapping image is in Fig. 3C, where red parts indicate mapped areas (*i.e.*, spectra of the red areas match with the PS reference library). The remaining panels show images of *D. magna* stained with different concentrations of stain: Fig. 3D and E have been stained with 5% H&E, Fig. 3F and G have been stained with 10% H&E, Fig. 3H and I have been stained with 25% H&E, Fig. 3J and K have been stained with 50% H&E, and Fig. 3L and M have been stained with 100% H&E. Fig. 3C, E, G, I, K and M are the spectral angle mapping images where red parts indicate mapped areas (scale bar: 10 μm). Green boxes on Fig. 3B, D, F, H, J, and L indicate where the biomass spectra for each staining concentration were taken from.

(Fig. S4). For example, when PS particles were stained with 50% and 100% H&E, the plastic spectrum red shifted to 614 nm (Fig. S4A). It's noted that despite this, the stained PS particles do not exhibit a major change in their spectral shape, thus ensuring the detection of nanoplastics with the Spectral Angle Mapping tool (Fig. 3K and M). The use of 25% H&E resulted in adequate changes to the biomass spectra compared to the control (0% stain) while using a minimal amount of stain. That is, 25% H&E stain resulted in a change in the spectra shape and a red shift in the peak wavelength, similar to using 50% and 100% H&E staining. Thus, to minimize the potential staining of plastic particles, 25% v/v H&E was selected as the optimal concentration for the remainder of this study. Additional replicates of this experiment at different ratios of H&E stain are shown in Fig. S5 and S6. Table S1 shows the average peak wavelength for biomass at each staining concentration.

For each staining concentration, the total number of particles, the correctly detected particles (true positives), the missed particles (false negatives), and the false positives were manually counted (Table S2). The 0% and 5% H&E staining concentrations resulted in a considerable amount of biomass being incorrectly detected as particles. For this reason, it was not possible to calculate the percentage of false positives. Hence, 0% and 5% staining were considered insufficient in differentiating between biomass and plastic particles. Based on the manual counts, it can be observed that 25% H&E staining concentration results in the optimum conditions for differentiating between biomass and plastic particles. Although 0% and 5% staining results in more true positives than the 25% H&E stain, the 25% concentration results in significantly fewer false positives. Furthermore, 25% H&E stain results in fewer false negatives than 50% and 100% H&E stain, which can be attributed to some staining of plastic particles at high H&E concentrations. Based on Table S2, 25% H&E was selected as the optimum staining concentration for this study.

The average spectrum of the spherical particles observed in the 25% H&E-stained histological slice was compared with the average spectrum of reference, unstained PS, as shown in
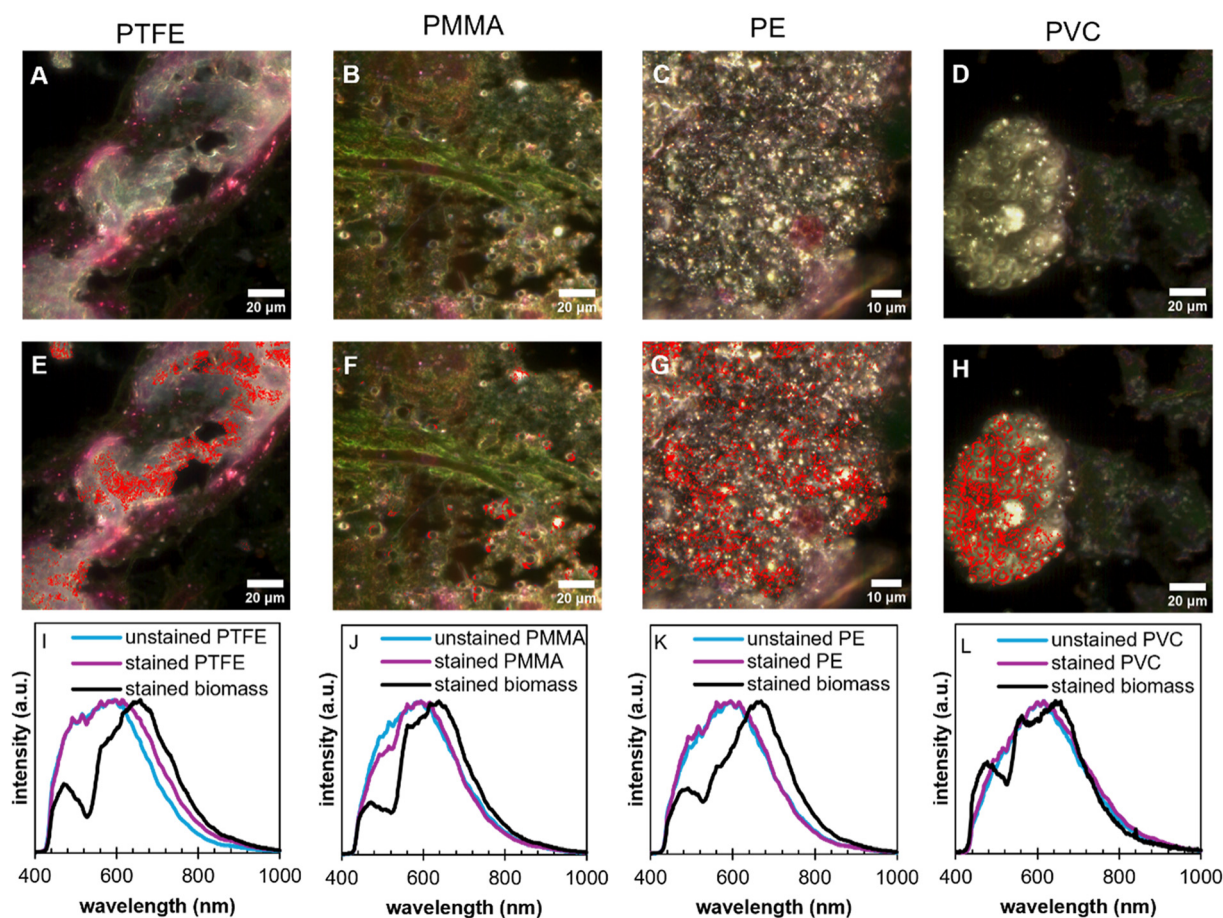
Fig. 4 The darkfield images of *D. magna* exposed to (A) 0.1 ppm of 200 nm PTFE, (B) 1 ppm of 1–10 μm PMMA, (C) 1 ppm of 3 μm PE, and (D) 10 ppm of 63 μm PVC are shown in the first row. In the second row, corresponding red pixels matched by the Spectral Angle Mapping tool for (E) PTFE, (F) PMMA, (G) PE, and (H) PVC are shown. The last row shows the control and stained polymer spectra of (I) PTFE, (J) PMMA, (K) PE, and (L) PVC. The peak wavelength of PTFE, PMMA, PE, and PVC within the sample is 596 nm, 595 nm, 596 nm, and 615 nm, respectively, whereas the control (unstained) PTFE, PMMA, PE, and PVC is 595 nm, 594 nm, 596 nm, and 615 nm, respectively. The reference spectrum for the unstained plastic particles (blue curve) is the same in all replicates.

Fig. S7. The lack of significant red shifting in the spectra of the stained particles enables matching of the particles by the Spectral Angle Mapping tool with the reference library for the PS particles. Three histological slices of a *D. magna*, which was not exposed to plastic particles (control sample), were also evaluated, where no signals characteristic to plastic particles were observed (a representative slice is shown in Fig. S8).

Demonstration with different plastic types, sizes, and concentrations

PS, PE, PMMA, PVC, and PTFE particles were exposed to the staining protocol and mapped using their respective reference library to confirm that H&E staining at a concentration of 25% v/v does not label different plastic types. Visual inspection of Fig. S9 indicates that 25% v/v H&E staining does not noticeably stain PS, PE, PMMA, PTFE, and PVC. The negligible extent of staining is evident by the shape of the polymer spectrum and peak maxima remaining unchanged before and after staining for PS, PVC, PE, and PTFE (Fig. S9K–S9M and S9O), resulting in accurate detection of those particles (Fig. S9F–S9H and S9J). However, staining resulted in a minor change in the spectrum shape for PMMA particles; thus, only a portion of the PMMA particles were mapped in Fig. S9I. Additional replicates of staining the different polymers with 25% H&E are presented in Fig. S10 and S11. In these two replicates, the shape of the spectrum for PMMA appears less affected by the staining.

D. magna was separately exposed to PTFE, PMMA, PE, and PVC particles. Spectral angle mapping successfully detected the ingested PTFE, PMMA, PE, and PVC plastic particles within the organism (Fig. 4). PMMA and PVC treatment conditions utilized particles of uniform spherical shape, enabling us to validate the Spectral Angle Mapping tool's ability to detect plastic particles. However, PE treatment conditions did not utilize particles of spherical shape as the UV-treated particles became irregular in shape and the PTFE treatment used small 200 nm particles, therefore it is challenging to confirm that the Spectral Angle Mapping tool has correctly detected particles and not biomass. Hence, to validate the procedure, optical photothermal infrared (O-PTIR) spectroscopy was used to confirm that the detected PE and PTFE were correctly mapped (Fig. S12).[63] In Fig. S12I and S12K, the IR spectra of various points on the histological slice confirm that the Spectral Angle Mapping tool was accurate in mapping PTFE and PE, respectively. IR spectra of the unmapped regions were also acquired, and it was determined to be biomass (Fig. S12J and S12L). Method validation was also carried out with O-PTIR for the PMMA, PVC and PS exposed *D. magna* (Fig. S13 and S14). With respect to the PMMA particles, while the majority were readily detected, some particles only had a portion that was detected by the mapping tool because the H&E stain can affect the shape of the PMMA spectrum (Fig. 4J and S9N). This could be due to the fact that PMMA is the least hydrophobic polymer among

the ones used in this study.[64] This may limit the application of this method for the detection of PMMA particles in biological samples. Further optimization of the staining protocol can be explored in future work, such as using different stain concentrations and types of stains for various plastic types. Despite this, the Spectral Angle Mapping is sufficient for rapid detection of PMMA particles within the organism (Fig. 4F). Additional examples of images for the detection of PTFE, PMMA, PE and PVC within *D. magna* can be observed in Fig. S15 and S16.

It is important to note that the depth of field plays a vital role in detecting plastic particles in the histological slices. For example, one study expressed concern that particles can shift or be dislodged from the sample when obtaining histological slices.[49] Aramendia *et al.* suggested that the observation of particles embedded within the biomass confirms the localization of particles in an area.[65] Similarly, in our study, nanoplastics were observed at various focal depths in the histological slice (Fig. S17 and S18), indicating that they are embedded within the biomass. This suggests that the detected nanoplastics are, in fact, localized in the
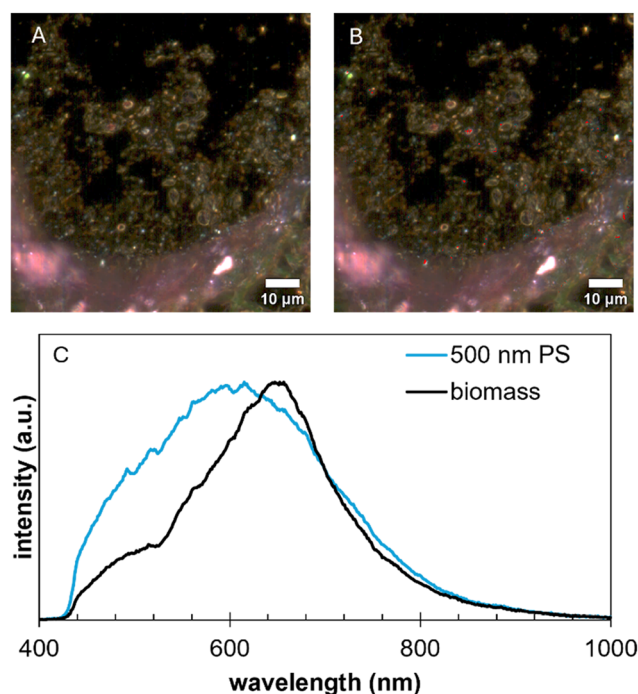

Fig. 5 Detection of ingested 500 nm PS at an exposure concentration of 0.01 ppm in *D. magna*. Histological slices were stained with 25% H&E stain. Fig. 5A is the darkfield image acquired on the EDF-HSI microscope of a 20 μm thick histological slice of *D. magna* exposed to 500 nm PS at 0.01 ppm. Fig. 5B is the corresponding spectral angle mapping image, which shows the detection of PS particles in red. In Fig. 5C, the blue curve is the average normalized spectrum of 50 pixels of plastic particles, and the black curve shows the average normalized spectrum of 50 pixels of biomass from Fig. 5A. The average normalized peak wavelength for 500 nm PS and biomass is 615 nm and 656 nm, respectively. Fig. 5A and B's brightness was increased by 44%, contrast decreased by 17%, and sharpness increased by 20% to improve visualization. Original images can be provided upon request.

gut rather than transported or dislodged during slicing by the blade.

To challenge this method further, *D. magna* was exposed to small nanoplastics (500 nm PS) at 0.01 ppm (Fig. 5). Although it is difficult to visually confirm 500 nm particles within a histological slice, Spectral Angle Mapping enables the detection of the smaller nanoplastics within a sample using the proposed methodology. This is due to the resolution of the EDF-HSI microscope enabling visualization of plastic particles as small as 100 nm in clean matrices.[47] However, the practical detection limit in this work refers to the smallest particle size that can be reliably resolved as discrete particles within the *D. magna* using the current methodology. Although smaller particles can be visualized in clean matrices, confident *in situ* resolution in biological samples is currently limited to ~500 nm under our conditions. Hence, further work must be carried out to detect nanoplastics smaller than 500 nm within whole organisms. Nonetheless, localizing nanoplastics as small as 500 nm within biological samples is advantageous compared to other characterization techniques, such as micro-Raman spectroscopy or conventional HSI (Table S3). Additional examples of detecting 500 nm PS in *D. magna* at an exposure concentration of 0.01 ppm can be observed in Fig. S21 and S22. The ability to detect microplastics and nanoplastics at lower concentrations is relevant to certain environmental conditions, as shown by Shi *et al.*, who found that nanoplastic concentrations in certain freshwater environments can range from 0.0003 to 0.433 ppm.[56]

Conclusion

This work proposes a qualitative method to detect microplastics and nanoplastics within a whole organism using hyperspectral imaging and histological techniques. H&E stain is used to selectively label biomass, thereby changing its spectral signature. This allows for spectral angle mapping to discriminate between plastic particles and biomass within a histological slice, while preserving the spatial distribution of particles. This study demonstrated the applicability of the method to different plastic types, which can improve our understanding of the impact, toxicity, and fate of a broad range of nanoplastics. Moreover, recent studies implement lower exposure concentrations but often rely on fluorescently labeled particles to visualize ingested particles.[66–68] The method proposed here demonstrates the detection of nanoplastics as small as 500 nm at low exposure concentrations, such as 0.01 ppm, which can enable researchers to implement lower exposure concentrations in controlled ecotoxicology experiments. This will improve the understanding of the toxicological impact of a wider range of nanoplastics at environmentally relevant concentrations.[56,67]

The proposed methodology expands on previous studies by enabling the detection of smaller plastic particles at environmentally relevant concentrations with the possibility of studying samples collected from the environment. For instance, Benito-Kaesbach *et al.*[49] proposed a protocol utilizing a cryotome and Raman spectroscopy to detect pre-labelled 1 μm PS microbeads within mussel tissue. A similar approach was reported by Collard *et al.*,[61] where cryotome sections of anchovies sampled from the Mediterranean Sea were analyzed for microplastics using Raman spectroscopy. The advantage of the proposed method lies in the detection of label-free particles, including nanoplastics, which have been overlooked in the literature. While our approach does not allow us to differentiate between different plastic types, advances are being made by combining machine learning techniques with hyperspectral data to improve the detection and identification of microplastics and nanoplastics.[69–71] Future work can focus on using machine learning techniques to differentiate polymer types in biological matrices using EDF-HSI.

The proposed method can also be used to quickly screen for plastic particles in samples collected from the environment. For instance, Collard *et al.* analyzed plastic particles ingested by anchovies collected from the environment by dissecting the liver, followed by cryotomy and imaging using Raman spectroscopy.[61] It is important to note that not all organisms can directly be sectioned using conventional cryotomes as they may not fit inside the instrument. In these cases, the organism would require dissection to study specific parts, as demonstrated by Collard *et al.*[61]

Environmental plastic particles would also undergo weathering, such as UV exposure. Preliminary results indicate that UV-exposed 500 nm PS particles can be detected by the Spectral Angle Mapping tool, suggesting that UV-weathering may not affect the ability to detect these particles (Fig. S23). However, the spectra of biofilm-coated nanoplastics would likely differ from those of pristine plastics, which will impact the ability of the spectral angle mapping tool to detect such particles. Future work can also focus on utilizing machine learning models to more effectively differentiate between biofilm-coated plastic particles and organism tissue.

As described in Table S3, EDF-HSI can achieve sub-micron detection in controlled matrices (reported down to 100 nm), whereas this study reports ~500 nm as the practical detection limit in a biological matrix. EDF-HSI also offers a faster image acquisition for higher throughput over other non-destructive tools, such as O-PTIR. Thus, the proposed method is a promising tool to quickly detect the presence of localized plastic particles in the gut of freshwater organisms, such as *D. magna*.

Nonetheless, this method does have its limitations. For instance, acquiring thick histological slices (20 μm) results in some plastic particles being out of focus, blocked by biomass, or embedded within the tissue.[49,61,65] To overcome this challenge, images at different depths of focus can be acquired to take into account unfocused particles (Fig. S17 and S18). Alternatively, thinner histological slices can also be acquired, which may result in losing some integrity of the organism's structure (Fig. S19 and S20). We note that dye

staining may reduce detection sensitivity for certain polymers in the current workflow (*e.g.*, PMMA), likely due to staining-induced spectral changes. Future work will focus on polymer-specific staining/optimization for different polymer types. Additionally, the Spectral Angle Mapping tool is unable to differentiate between plastic types because the spectra are similar in shape and peak wavelengths for different plastic types (PS – 595 nm, PVC – 615 nm, PTFE – 595 nm, PMMA – 594 nm, and PE – 596 nm). Since hyperspectral data acquired from this method uses a halogen light source emitting visible light, two pixels with a similar RGB profile will result in a similar spectrum. Hence, the proposed methodology should be viewed as a detection and localization tool, rather than a polymer identification method in its present form. Although the inability to differentiate between plastic types will affect the utility of this method to differentiate plastic particles in environmental samples containing mixed plastics, it can still be used to quickly screen for plastic particles in complex matrices. Therefore, this method is best suited for mapping particle presence and distribution, while polymer identification should be performed using complementary spectroscopy (*e.g.*, O-PTIR, FTIR, Raman) on selected particles. In fact, a combination of different imaging techniques can lead to more accurate plastic particle identification.[25] The non-destructive nature of this method allows for further analysis of processed samples using additional techniques, such as Raman, FTIR, or O-PTIR microscopy, which can identify the polymer type. Although the spectral data cannot be used to identify the different plastic types within a sample, this method proves to be an efficient procedure to rapidly detect nanoplastics as small as 500 nm at environmentally relevant concentrations. Furthermore, the post-exposure staining methodology[72] presented in this work can be especially useful for toxicology studies, eliminating the need to use labeled plastic particles in organism exposures. Overall, this methodology will be a useful technique to improve our understanding of nanoplastic localization in organisms, thereby advancing our knowledge of the potential impacts of this contaminant.

Author contributions

A. S. developed the methodology and performed the experiments with assistance from J. R. M. and E. G.; A. S., J. R. M., and N. T. contributed to the study's conceptualization. All co-authors contributed to the manuscript drafting and editing.

Conflicts of interest

All authors confirm that there are no conflicts to declare.

Data availability

The data that support the findings of this study, including original image files, and hyperspectral data, are deposited into a publicly available repository, which can be accessed here: https://doi.org/10.5281/zenodo.18601195.

Supplementary information: Reference images of PS, PVC, PE, PMMA, and PTFE acquired using EDF-HSI; assessment of staining on different polymer types; replicates of detection of nanoplastics at different H&E staining concentrations and the corresponding average peak wavelengths; statistical analysis of the spectra angle mapping tool's detection of nanoplastics; comparison of reference PS and PS within biomass; detection of plastic particles in unexposed *Daphnia magna* as control; mapping and detection of reference PS, PVC, PE, PMMA, and PTFE after staining with 25% H&E; method validation using O-PTIR analysis of PE, PTFE, PVC, PMMA, and PS within histological slice; replicates of detecting different polymers within *D. magna*; analysis and discussion of acquiring vertical stack images of one histological slice; comparison of detecting particles within 20 μm and 10 μm thick histological slices; replicates of detecting 500 nm PS within *Daphnia magna*; preliminary results of detecting UV-weathered nanoplastics; and comparing EDF-HSI to other microplastic and nanoplastic characterization techniques. See DOI: https://doi.org/10.1039/d5en00992h.

References

1 J. P. G. L. Frias and R. Nash, Microplastics: Finding a consensus on the definition, *Mar. Pollut. Bull.*, 2019, **138**, 145–147.

2 J. Gigault, A. t. Halle, M. Baudrimont, P.-Y. Pascal, F. Gauffre, T.-L. Phi, H. El Hadri, B. Grassl and S. Reynaud, Current opinion: What is a nanoplastic?, *Environ. Pollut.*, 2018, **235**, 1030–1034.

3 B. Zhang, J. Chao, L. Chen, L. Liu, X. Yang and Q. Wang, Research progress of nanoplastics in freshwater, *Sci. Total Environ.*, 2021, **757**, 143791.

4 S.-A. Strungaru, R. Jijie, M. Nicoara, G. Plavan and C. Faggio, Micro- (nano) plastics in freshwater ecosystems: Abundance, toxicological impact and quantification methodology, *TrAC, Trends Anal. Chem.*, 2019, **110**, 116–128.

5 Z. Wang, Y. Qin, W. Li, W. Yang, Q. Meng and J. Yang, Microplastic contamination in freshwater: first observation in Lake Ulansuhai, Yellow River Basin, China, *Environ. Chem. Lett.*, 2019, **17**, 1821–1830.

6 A. Alfaro-Núñez, D. Astorga, L. Cáceres-Farías, L. Bastidas, C. Soto Villegas, K. Macay and J. H. Christensen, Microplastic pollution in seawater and marine organisms across the Tropical Eastern Pacific and Galápagos, *Sci. Rep.*, 2021, **11**, 6424.

7 S. Moon, L. M. A. Martin, S. Kim, Q. Zhang, R. Zhang, W. Xu and T. Luo, Direct observation and identification of nanoplastics in ocean water, *Sci. Adv.*, 2024, **10**, eadh1675.

8 D. Materić, E. Ludewig, D. Brunner, T. Röckmann and R. Holzinger, Nanoplastics transport to the remote, high-altitude Alps, *Environ. Pollut.*, 2021, **288**, 117697.

9 Y. Zhang, T. Gao, S. Kang, S. Allen, X. Luo and D. Allen, Microplastics in glaciers of the Tibetan Plateau: Evidence for the long-range transport of microplastics, *Sci. Total Environ.*, 2021, **758**, 143634.

10 H. Wang, Q. Wang, M. Lv, J. Li, X. Zhao, Z. Song, X. Wang, J. You, Y. Wang and L. Chen, Marine micro(nano)plastics determination and its environmental toxicity evaluation, *TrAC, Trends Anal. Chem.*, 2023, **168**, 117332.

11 F. Ribeiro, E. D. Okoffo, J. W. O'Brien, S. O'Brien, J. M. Harris, S. Samanipour, S. Kaserzon, J. F. Mueller, T. Galloway and K. V. Thomas, Out of sight but not out of mind: Size fractionation of plastics bioaccumulated by field deployed oysters, *J. Hazard. Mater. Lett.*, 2021, **2**, 100021.

12 K. Yin, Y. Wang, H. Zhao, D. Wang, M. Guo, M. Mu, Y. Liu, X. Nie, B. Li and J. Li, A comparative review of microplastics and nanoplastics: Toxicity hazards on digestive, reproductive and nervous system, *Sci. Total Environ.*, 2021, **774**, 145758.

13 J. Gigault, H. El Hadri, B. Nguyen, B. Grassl, L. Rowenczyk, N. Tufenkji, S. Feng and M. Wiesner, Nanoplastics are neither microplastics nor engineered nanoparticles, *Nat. Nanotechnol.*, 2021, **16**, 501–507.

14 Y. Ji, L. Chen, Y. Wang, J. Zhang, Y. Yu, M. Wang, X. Wang, W. Liu, B. Yan, L. Xiao, X. Song, C. Lv and L. Chen, Realistic Nanoplastics Induced Pulmonary Damage via the Crosstalk of Ferritinophagy and Mitochondrial Dysfunction, *ACS Nano*, 2024, **18**, 16790–16807.

15 L. Liu, K. Xu, B. Zhang, Y. Ye, Q. Zhang and W. Jiang, Cellular internalization and release of polystyrene microplastics and nanoplastics, *Sci. Total Environ.*, 2021, **779**, 146523.

16 V. K. Sharma, X. Ma, E. Lichtfouse and D. Robert, Nanoplastics are potentially more dangerous than microplastics, *Environ. Chem. Lett.*, 2023, **21**, 1933–1936.

17 A. T. B. Guimarães, F. N. Estrela, A. S. d. L. Rodrigues, T. Q. Chagas, P. S. Pereira, F. G. Silva and G. Malafaia, Nanopolystyrene particles at environmentally relevant concentrations causes behavioral and biochemical changes in juvenile grass carp (Ctenopharyngodon idella), *J. Hazard. Mater.*, 2021, **403**, 123864.

18 K. Yin, Y. Wang, H. Zhao, D. Wang, M. Guo, M. Mu, Y. Liu, X. Nie, B. Li, J. Li and M. Xing, A comparative review of microplastics and nanoplastics: Toxicity hazards on digestive, reproductive and nervous system, *Sci. Total Environ.*, 2021, **774**, 145758.

19 M. Velimirovic, K. Tirez, S. Verstraelen, E. Frijns, S. Remy, G. Koppen, A. Rotander, E. Bolea-Fernandez and F. Vanhaecke, Mass spectrometry as a powerful analytical tool for the characterization of indoor airborne microplastics and nanoplastics, *J. Anal. At. Spectrom.*, 2021, **36**, 695–705.

20 A. Käppler, D. Fischer, S. Oberbeckmann, G. Schernewski, M. Labrenz, K.-J. Eichhorn and B. Voit, Analysis of environmental microplastics by vibrational microspectroscopy: FTIR, Raman or both?, *Anal. Bioanal. Chem.*, 2016, **408**, 8377–8391.

21 L. Cabernard, L. Roscher, C. Lorenz, G. Gerdts and S. Primpke, Comparison of Raman and Fourier Transform Infrared Spectroscopy for the Quantification of Microplastics in the Aquatic Environment, *Environ. Sci. Technol.*, 2018, **52**, 13279–13288.

22 B. N. Vinay Kumar, L. A. Löschel, H. K. Imhof, M. G. J. Löder and C. Laforsch, Analysis of microplastics of a broad size range in commercially important mussels by combining FTIR and Raman spectroscopy approaches, *Environ. Pollut.*, 2021, **269**, 116147.

23 S. Adhikari, V. Kelkar, R. Kumar and R. U. Halden, Methods and challenges in the detection of microplastics and nanoplastics: a mini-review, *Polym. Int.*, 2022, **71**, 543–551.

24 D. Xie, H. Fang, X. Zhao, Y. Lin and Z. Su, Identification of microplastics and nanoplastics in environmental water by AFM-IR, *Anal. Chim. Acta*, 2025, **1354**, 343992.

25 A. Faltynkova, G. Johnsen and M. Wagner, Hyperspectral imaging as an emerging tool to analyze microplastics: A systematic review and recommendations for future development, *Microplast. Nanoplast.*, 2021, **1**, 13.

26 A. Gebejes, B. Hrovat, D. Semenov, B. Kanyathare, T. Itkonen, M. Keinänen, A. Koistinen, K. E. Peiponen and M. Roussey, Hyperspectral imaging for identification of irregular-shaped microplastics in water, *Sci. Total Environ.*, 2024, **944**, 173811.

27 L. Fiore, S. Serranti, C. Mazziotti, E. Riccardi, M. Benzi and G. Bonifazi, Classification and distribution of freshwater microplastics along the Italian Po river by hyperspectral imaging, *Environ. Sci. Pollut. Res.*, 2022, **29**, 48588–48606.

28 Y. Zhang, X. Wang, J. Shan, J. Zhao, W. Zhang, L. Liu and F. Wu, Hyperspectral Imaging Based Method for Rapid Detection of Microplastics in the Intestinal Tracts of Fish, *Environ. Sci. Technol.*, 2019, **53**, 5151–5158.

29 S. Piarulli, C. Malegori, F. Grasselli, L. Airoldi, S. Prati, R. Mazzeo, G. Sciutto and P. Oliveri, An effective strategy for the monitoring of microplastics in complex aquatic matrices: Exploiting the potential of near infrared hyperspectral imaging (NIR-HSI), *Chemosphere*, 2022, **286**, 131861.

30 W. Ai, S. Liu, H. Liao, J. Du, Y. Cai, C. Liao, H. Shi, Y. Lin, M. Junaid, X. Yue and J. Wang, Application of hyperspectral imaging technology in the rapid identification of microplastics in farmland soil, *Sci. Total Environ.*, 2022, **807**, 151030.

31 C. Zhu, Y. Kanaya, R. Nakajima, M. Tsuchiya, H. Nomaki, T. Kitahashi and K. Fujikura, Characterization of microplastics on filter substrates based on hyperspectral imaging: Laboratory assessments, *Environ. Pollut.*, 2020, **263**, 114296.

32 C. Vidal and C. Pasquini, A comprehensive and fast microplastics identification based on near-infrared hyperspectral imaging (HSI-NIR) and chemometrics, *Environ. Pollut.*, 2021, **285**, 117251.

33 B. Nguyen, D. Claveau-Mallet, L. M. Hernandez, E. G. Xu, J. M. Farner and N. Tufenkji, Separation and Analysis of Microplastics and Nanoplastics in Complex Environmental Samples, *Acc. Chem. Res.*, 2019, **52**, 858–866.

34 A. Karami, A. Golieskardi, C. K. Choo, N. Romano, Y. B. Ho and B. Salamatinia, A high-performance protocol for extraction of microplastics in fish, *Sci. Total Environ.*, 2017, **578**, 485–494.

35 M. Scheurer and M. Bigalke, Microplastics in Swiss Floodplain Soils, *Environ. Sci. Technol.*, 2018, **52**, 3591–3598.

36 M.-T. Nuelle, J. H. Dekiff, D. Remy and E. Fries, A new analytical approach for monitoring microplastics in marine sediments, *Environ. Pollut.*, 2014, **184**, 161–169.

37 E. G. Karakolis, B. Nguyen, J. B. You, C. M. Rochman and D. Sinton, Fluorescent Dyes for Visualizing Microplastic Particles and Fibers in Laboratory-Based Studies, *Environ. Sci. Technol. Lett.*, 2019, **6**, 334–340.

38 Y. Ji, C. Wang, Y. Wang, L. Fu, M. Man and L. Chen, Realistic polyethylene terephthalate nanoplastics and the size- and surface coating-dependent toxicological impacts on zebrafish embryos, *Environ. Sci.: Nano*, 2020, **7**, 2313–2324.

39 T. Stanton, M. Johnson, P. Nathanail, R. L. Gomes, T. Needham and A. Burson, Exploring the Efficacy of Nile Red in Microplastic Quantification: A Costaining Approach, *Environ. Sci. Technol. Lett.*, 2019, **6**, 606–611.

40 G. Malafaia, T. M. da Luz, M. A. I. Ahmed, S. Karthi and A. P. da Costa Araújo, When toxicity of plastic particles comes from their fluorescent dye: a preliminary study involving neotropical Physalaemus cuvieri tadpoles and polyethylene microplastics, *J. Hazard. Mater. Adv.*, 2022, **6**, 100054.

41 R. Fakhrullin, L. Nigamatzyanova and G. Fakhrullina, Dark-field/hyperspectral microscopy for detecting nanoscale particles in environmental nanotoxicology research, *Sci. Total Environ.*, 2021, **772**, 145478.

42 A. R. Badireddy, M. R. Wiesner and J. Liu, Detection, Characterization, and Abundance of Engineered Nanoparticles in Complex Waters by Hyperspectral Imagery with Enhanced Darkfield Microscopy, *Environ. Sci. Technol.*, 2012, **46**, 10081–10088.

43 T. Théoret and K. J. Wilkinson, Evaluation of enhanced darkfield microscopy and hyperspectral analysis to analyse the fate of silver nanoparticles in wastewaters, *Anal. Methods*, 2017, **9**, 3920–3928.

44 P. Zamora-Perez, D. Tsoutsi, R. Xu and P. Rivera_Gil, Hyperspectral-Enhanced Dark Field Microscopy for Single and Collective Nanoparticle Characterization in Biological Environments, *Materials*, 2018, **11**, 243.

45 T. L. Botha, K. Boodhia and V. Wepener, Adsorption, uptake and distribution of gold nanoparticles in Daphnia magna following long term exposure, *Aquat. Toxicol.*, 2016, **170**, 104–111.

46 I. Ishmukhametov, L. Nigamatzyanova, G. Fakhrullina and R. Fakhrullin, Label-free identification of microplastics in human cells: dark-field microscopy and deep learning study, *Anal. Bioanal. Chem.*, 2022, **414**, 1297–1312.

47 L. Nigamatzyanova and R. Fakhrullin, Dark-field hyperspectral microscopy for label-free microplastics and nanoplastics detection and identification in vivo: A Caenorhabditis elegans study, *Environ. Pollut.*, 2021, **271**, 116337.

48 A. Batel, L. Baumann, C. C. Carteny, B. Cormier, S. H. Keiter and T. Braunbeck, Histological, enzymatic and chemical analyses of the potential effects of differently sized microplastic particles upon long-term ingestion in zebrafish (Danio rerio), *Mar. Pollut. Bull.*, 2020, **153**, 111022.

49 A. Benito-Kaesbach, J. M. Amigo, U. Izagirre, N. Garcia-Velasco, L. Arévalo, A. Seifert and K. Castro, Misinterpretation in microplastic detection in biological tissues: When 2D imaging is not enough, *Sci. Total Environ.*, 2023, **876**, 162810.

50 R. A. B. Drury, E. A. Wallington and S. R. Cameron, *Carleton's histological technique*, London, 1967.

51 R. D. Lillie, *Histopathologic technic and practical histochemistry*, 1954.

52 A. H. Fischer, K. A. Jacobson, J. Rose and R. Zeller, Hematoxylin and eosin staining of tissue and cell sections, *Cold Spring Harb. Protoc.*, 2008, **2008**, pdb.prot4986.

53 M. Hamed, H. A. M. Soliman, A. E. A. Badrey and A. G. M. Osman, Microplastics induced histopathological lesions in some tissues of tilapia (Oreochromis niloticus) early juveniles, *Tissue Cell*, 2021, **71**, 101512.

54 K. Pelegrini, T. C. B. Pereira, T. G. Maraschin, L. D. S. Teodoro, N. R. D. S. Basso, G. L. B. De Galland, R. A. Ligabue and M. R. Bogo, Micro- and nanoplastic toxicity: A review on size, type, source, and test-organism implications, *Sci. Total Environ.*, 2023, **878**, 162954.

55 O. Pikuda, E. R. Dumont, S. Matthews, E. G. Xu, D. Berk and N. Tufenkji, Sub-lethal effects of nanoplastics upon chronic exposure to Daphnia magna, *J. Hazard. Mater. Adv.*, 2022, **7**, 100136.

56 C. Shi, Z. Liu, B. Yu, Y. Zhang, H. Yang, Y. Han, B. Wang, Z. Liu and H. Zhang, Emergence of nanoplastics in the aquatic environment and possible impacts on aquatic organisms, *Sci. Total Environ.*, 2024, **906**, 167404.

57 P. Dey, in *Basic and Advanced Laboratory Techniques in Histopathology and Cytology*, Springer Singapore, Singapore, 2018, pp. 69–79, DOI: 10.1007/978-981-10-8252-8_8.

58 A. T. Feldman and D. Wolfe, in *Histopathology: Methods and Protocols*, ed. C. E. Day, Springer New York, New York, NY, 2014, pp. 31–43, DOI: 10.1007/978-1-4939-1050-2_3.

59 B. Nguyen and N. Tufenkji, Single-Particle Resolution Fluorescence Microscopy of Nanoplastics, *Environ. Sci. Technol.*, 2022, **56**, 6426–6435.

60 C. Gonçalves, M. Martins, M. H. Costa and P. M. Costa, Development of a method for the detection of polystyrene microplastics in paraffin-embedded histological sections, *Histochem. Cell Biol.*, 2018, **149**, 187–191.

61 F. Collard, B. Gilbert, P. Compère, G. Eppe, K. Das, T. Jauniaux and E. Parmentier, Microplastics in livers of European anchovies (Engraulis encrasicolus, L.), *Environ. Pollut.*, 2017, **229**, 1000–1005.

62 M. A. Kryuchkova, I. R. Ishmukhametov, Y. A. Frank, A. V. Simakova, V. V. Yartsev, D. A. Nadueva, A. A. Varenitsina, Y. V. Andreeva and R. F. Fakhrullin, Fluorescence-Free Tracking of Polystyrene Microplastics in Mosquito Larvae Using Dark-Field Hyperspectral Microscopy, *Colloid J.*, 2024, **86**, 466–475.

63 J.-R. Macairan, A. Saherwala, F. Li, F. Monteil-Rivera and N. Tufenkji, Label-Free Identification and Imaging of Microplastic and Nanoplastic Bioxptake Using Optical Photothermal Infrared Microspectroscopy, *Environ. Sci. Technol.*, 2025, **59**(30), 15612–15622.

64 J. Sena, L. O. Johannissen, J. J. Blaker and S. Hay, A Machine Learning Model for the Prediction of Water Contact Angles on Solid Polymers, *J. Phys. Chem. B*, 2025, **129**, 2739–2745.

65 J. Aramendia, N. García-Velasco, J. M. Amigo, U. Izagirre, A. Seifert, M. Soto and K. Castro, Evidence of internalized microplastics in mussel tissues detected by volumetric Raman imaging, *Sci. Total Environ.*, 2024, **914**, 169960.

66 A. Banerjee, L. O. Billey and W. L. Shelver, Uptake and toxicity of polystyrene micro/nanoplastics in gastric cells: Effects of particle size and surface functionalization, *PLoS One*, 2022, **16**, e0260803.

67 S. Lasee, J. Mauricio, W. A. Thompson, A. Karnjanapiboonwong, J. Kasumba, S. Subbiah, A. N. Morse and T. A. Anderson, Microplastics in a freshwater environment receiving treated wastewater effluent, *Integr. Environ. Assess. Manage.*, 2017, **13**, 528–532.

68 M. Sendra, P. Pereiro, M. P. Yeste, L. Mercado, A. Figueras and B. Novoa, Size matters: Zebrafish (Danio rerio) as a model to study toxicity of nanoplastics from cells to the whole organism, *Environ. Pollut.*, 2021, **268**, 115769.

69 L. Xie, M. Ma, Q. Ge, Y. Liu and L. Zhang, Machine Learning Advancements and Strategies in Microplastic and Nanoplastic Detection, *Environ. Sci. Technol.*, 2025, **59**, 8885–8899.

70 J. Shan, J. Zhao, Y. Zhang, L. Liu, F. Wu and X. Wang, Simple and rapid detection of microplastics in seawater using hyperspectral imaging technology, *Anal. Chim. Acta*, 2019, **1050**, 161–168.

71 M. Seidel, C. Hutengs, J. Bauer, B. Schneider, M. Ortner, S. Thiele-Bruhn and M. Vohland, Efficient screening of microplastics in soils using hyperspectral imaging in the short-wave infrared range coupled with machine learning – A laboratory-based experiment, *Ecol. Indic.*, 2025, **173**, 113301.

72 J. R. Macairan, B. Nguyen, F. Li and N. Tufenkji, Tissue Clearing To Localize Microplastics via Three-Dimensional Imaging of Whole Organisms, *Environ. Sci. Technol.*, 2023, **57**, 8476–8483.